Ultrafast Chemistry of Nanoenergetic Materials Studied by Time−Resolved Infrared Spectroscopy: Aluminum Nanoparticles in Teflon

ARTICLE *in* THE JOURNAL OF PHYSICAL CHEMISTRY C · JUNE 2007

Impact Factor: 4.77 · DOI: 10.1021/jp072662h

3 AUTHORS, INCLUDING:

Dana D Dlott
University of Illinois, Urbana-Champaign
297 PUBLICATIONS **6,640** CITATIONS

SEE PROFILE

Ultrafast Chemistry of Nanoenergetic Materials Studied by Time-Resolved Infrared Spectroscopy: Aluminum Nanoparticles in Teflon

Mikhail A. Zamkov, Rusty W. Conner, and Dana D. Dlott*

School of Chemical Sciences, University of Illinois at Urbana−Champaign, Urbana, Illinois 61801

Received: April 4, 2007; In Final Form: May 12, 2007

Ultrafast mid-infrared (IR) spectroscopy is used to monitor chemical reactions initiated by flash-heating a nanoenergetic material consisting of 30 nm diameter Al nanoparticle fuel in a Teflon^{AF} oxidizer. Teflon^{AF} is a copolymer of tetrafluoroethylene (TFE) and 2,2-bis(trifluoromethyl)-4,5-difluoro-1,3-dioxole (dioxole), so Al can react with several different moieties. Transitions associated with CF_2 stretching of TFE or CFO stretching or CF_3 stretching of dioxole were monitored. The reactions of Al with CFO occurred with time constant $(k_1)^{-1} = 50$ (±20 ps); reactions of Al with CF_2 or CF_3 were more than 10 times slower, $(k_2)^{-1} = 0.7$ (±0.05 ns). An interesting frequency oscillation is seen in the 1148 cm^{-1} band, where the peak frequency undergoes a time-dependent shift from 1148 to 1155 cm^{-1} and then back to 1148 cm^{-1}. Due to the coincidence of CFO and CF_2 stretching transitions, this band in the copolymer represents an amalgamated vibration with amplitude on both TFE and dioxole. As concentration is varied from pure dioxole to pure TFE, the band blue-shifts. A kinetic scheme and a model for the concentration dependence of the amalgamated vibration frequency are developed, which show that the frequency oscillation is a consequence of the arrangement of reactants on the nanoscale, which creates two types of oxidizer. The type adjacent to the Al nanoparticle is in a region of high local fuel concentration, while the other type is too distant from the fuel to react.

1. Introduction

A great deal of excitement was created in the field of energetic materials by the introduction of nanotechnology.[1−3] Nanoenergetic materials can have an energy content more than twice as great as the best molecular explosives, and there are potentially more ways to control the energetic response via modifications in the nanostructure than with conventional materials,[3] for example, nitroaromatic molecules such as 2,4,6-trinitrotoluene (TNT). This paper is concerned with fast chemistry in one such nanoenergetic material, composed of nearly monodisperse 30 nm diameter Al nanoparticles having a native oxide passivation layer, embedded in a Teflon^{AF} oxidizer. An Al/Teflon mix has a theoretical heat of combustion of 21 kJ/cm^3, compared for instance to only 8 kJ/cm^3 for TNT.[1,3,4] Al/Teflon composites are also interesting since they can support multifunctional applications,[5] for instance, by serving as a structural element or weapon casing.

This paper is an investigation in detail of the fuel-oxidizer chemistries occurring in Al/Teflon^{AF} and the effects of nanostructure on these chemistries. Generally speaking, there are very few measurements exploring the reaction dynamics in the condensed phase of combusting or detonating energetic materials, due to the difficulties of probing molecular species engaged in fast reactions inside solid materials.[4] Our experiments[6−12] combine laser flash-heating with time-resolved spectroscopic probing. The first measurements of this sort on a similar nanoenergetic material, by Parker et al.,[13] combined flash-heating with nanosecond emission spectroscopy. In the present work we probe chemical reactions inside the combusting material using femtosecond IR spectroscopy. The scheme depicted in Figure 1 is used, which supports high repetition rate transient absorption measurements.

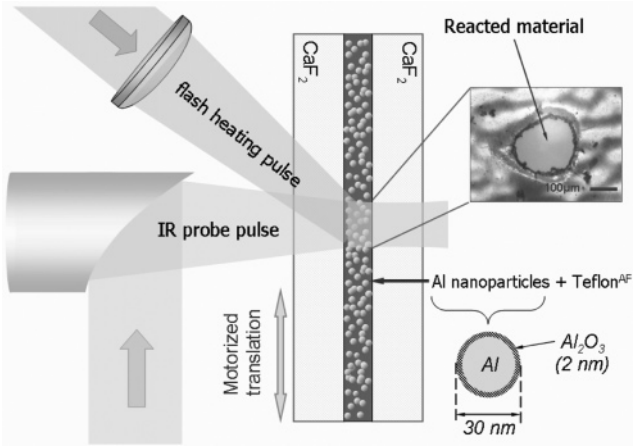

Figure 1. Schematic diagram of IR transient absorbance flash-heating measurements on Al nanoparticle-doped Teflon films. The samples used in this work were 18 wt % Al (30 nm, 2 nm oxide passivation) in Teflon^{AF} polymer.

The energetic reaction between Al and Teflon might be expressed in a greatly simplified way as,

$$Al + (^3/_2)CF_2 \rightarrow AlF_3 + (^3/_2)C$$

However, Teflon^{AF} is not simply poly(tetrafluoroethylene) (PTFE); it is a copolymer of tetrafluoroethylene (TFE) with a fluorinated group, 2,2-bis(trifluoromethyl)-4,5-difluoro-1,3-dioxole (hereafter TFE and dioxole). This copolymer can be dissolved in a fluorocarbon solvent and used to produce high optical quality thin films.

* Author to whom correspondence should be addressed.

10.1021/jp072662h CCC: $37.00
Published on Web 06/21/2007

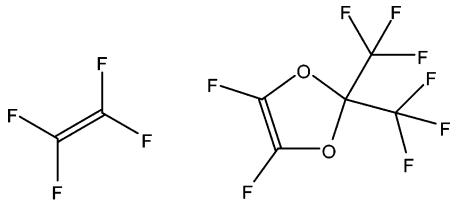

TFE dioxole

If it is assumed that a Teflon^{AF} copolymer is 66% mole fraction dioxole (see below) and that Al combusts to produce only AlF_3 and Al_2O_3 (which may not necessarily be the case), then the mass ratio for a stoichiometric mixture would be Teflon^{AF}:Al = 2.3:1.

Although the chemistry between Al and Teflon^{AF} is obviously complicated, we will discuss our results within a simplified framework. We use IR transient absorption spectroscopy to monitor the disappearance of transitions that can be associated with CF_2 stretching of TFE and CFO or CF_3 stretching of dioxole. Any of these bands will lose intensity when Al atoms react with an F atom of CF_2 or CF_3, or an O or F atom of CFO.

Besides the energetic chemistry discussed above, another important feature of this system results from the material nanostructure. Nanoenergetic materials belong to a class termed composite explosives or propellants, meaning they consist of separate fuel and oxidizer components, in contrast to, for example, TNT, where every molecule possesses both fuel and oxidizing moieties.

As depicted schematically in Figure 1, passivated Al nanoparticles will be flash-heated by a laser pulse. To better visualize the energetic process, in Figure 2 we present a time series of images obtained from our ultrafast microscopy system.[14,15] In these images the laser pulse duration was 100 ns and the Al/Teflon^{AF} layer was in contact with just one supporting window (i.e., the energetic material is the filling in an open-faced sandwich). In the IR experiments reported here, a much more powerful 120 ps duration flash-heating pulse is used[16] and the sample is fully confined between a pair of windows.

Flash-heating gives rise to a two-part reaction within the Al/Teflon sample.[7,11] First, hot Al breaks through its passivation layer[6] to react at the Al/Teflon interface. When the nanoparticle concentration is lower than that needed to consume all the Teflon oxidizer in the sample, which is the case here, reactions with Al are confined to local regions of Teflon surrounding each nanoparticle. Assuming the stoichiometry associated with the reaction above, and modeling these local regions as spherical shells surrounding a 30 nm diameter nanoparticle with a 2 nm oxide passivation layer,[7] this shell diameter should be $d_{sh} \approx 45$ nm. The energy within this region, which is mostly from the flash-heating pulse with a minor contribution from chemical reactions, generates a "blast wave",[7,17] that is, an expanding attenuating spherical shock front. This shock front depolymerizes the Teflon within a spherical region delimited by the distance where the shock strength drops below a critical value.[7] The diameter of the reaction volume that includes Al/Teflon reactions and shock-induced Teflon depolymerization is denoted d_{rxn}. As expected from this discussion, at a minimal flash-heating laser fluence just enough to initiate reactions, the reaction volume is about equal to the volume of the shell, $d_{rxn} \approx d_{sh}$.[7] Above this minimum, d_{rxn} increases with increasing fluence. In previous work with 30 nm Al at laser fluences 10 times greater than those used here, reaction distances d_{rxn} up to 400 nm were observed.[6,7,18]

In this paper we will concentrate on the mechanisms associated with the first part of this reaction, between a hot Al nanoparticle and its adjacent shell of Teflon^{AF}. The depolymerization phases of the flash-heating process will not be discussed. Teflon^{AF} is a high molecular weight polymer, and as long as depolymerization does not produce very small molecular weight fragments, the Teflon IR spectrum should be insensitive to the degree of polymerization. This insensitivity was verified by comparing a high molecular weight Teflon material to a lower molecular weight Zonyl material. The primary Teflon IR transitions in these two materials differed only by small peak shifts and line width changes that would be difficult for our transient IR apparatus to observe.

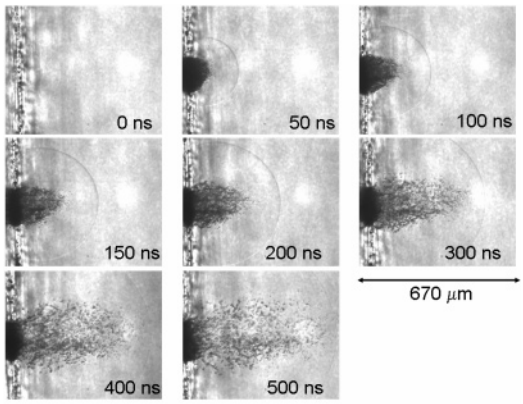

Figure 2. Time series of images obtained by flash-heating an Al/Teflon^{AF} thin film in an unconfined geometry, using a 100 ns duration 1064 nm laser pulse. The beam diameter is 50 μm and the pulse energy is 40 μJ. The images show the Al/Teflon^{AF} surface at far left. The flash-heating pulses are input from right to left. The images show the explosive ablation of material from the surface at the indicated times. The hemisphere is a blast wave in the air. Reproduced from ref 15. Copyright Materials Research Society.

In earlier work, nanoaluminum embedded in nitrocellulose (NC) oxidizer was studied by use of a time-resolved coherent anti-Stokes Raman scattering (CARS) probe.[6−9,11,19] With CARS we were able to monitor Al reactions with NC via the disappearance of signal from the nitrato (ONO_2) symmetric stretching vibration. However, CARS proved to have several limitations for this type of investigation: CARS signals were weak because Raman cross-sections are small; the visible pulses used for CARS measurements were scattered and attenuated by the metal nanoparticles, which limited us to nanoparticle loading less than 2 wt %; the CARS signals were deflected away from the detector by transient lensing related to shock wave generation and propagation;[20−22] and the visible emission burst associated with the fast reactions interfered with the visible CARS signal. For these reasons, we have not been successful in getting transient CARS spectra from Teflon-based nanoenergetics.

We have now developed a broadband dual-beam multichannel fast IR system that alleviates many of these problems. IR cross-sections are many orders of magnitude (typically 10^{10}) greater than Raman cross-sections. The longer-wavelength IR pulses are scattered and deflected much less than visible light, and IR probe pulses are much brighter than the emission burst from the sample. With this new IR system we are now able to elucidate details of the reactions of Teflon^{AF} with Al nanoparticles.

2. Experimental Section

A. Sample Preparation. Preparation of Al/Teflon^{AF} samples is similar to what was described earlier.[7,18] The Al particles obtained from Technanogy, Inc. (Santa Ana, CA), according

to the manufacturer's specifications had a nominal diameter of 30.2 (±3 nm) and an oxide layer 2 nm thick. In our samples the mass ratio of Teflon^{AF}/Al was 4.6 (i.e., the sample was 18% Al by weight). According to the discussion associated with eq 1, this is our best estimate of the amount of Al needed to consume 50% of the Teflon^{AF}. Al nanoparticles were suspended in ethanol and a small amount of a fluorinated surfactant, 1*H*,1*H*,2*H*,2*H*-perfluorodecyltriethoxysilane (Lancaster Synthesis), was added. The surfactant-treated nanoparticles were dried and then suspended in Fluorinert FC-77 fluorocarbon solvent (3M Corp.). To the nanoparticle suspension we added Teflon^{AF} 600 (DuPont), a 6% solution of Teflon^{AF} in a perfluorinated solvent.

The suspension was shaken and extensively sonicated prior to spin coating onto a CaF_2 window at 600 rpm. After drying, a film thickness of 3−4 μm was measured by profilometry. The dried film was covered with a second CaF_2 window to create the sandwich arrangement depicted in Figure 1. The sandwich was mounted on a two-axis motorized positioner. An acceleration and velocity profile could be downloaded to the positioning controller to raster the sample so that the laser operating at 100 pps always ignited a fresh spot.

B. Flash Heating. The flash heating process has been described in detail previously.[7,11,12] This technique employs 100 ps near-IR pulses, which are absorbed by Al nanoparticles but not by Teflon^{AF}, to create nanometric hot spots of Al vapor that are highly reactive toward Teflon. The near-IR pulses deposit energy into the skin layer of the metallic particles,[23] but 100 ps is longer than the time needed for thermal conduction into the interior of the nanoparticle, so the particles should be viewed as being uniformly heated throughout.[7,11,12] In previous works, 1053 nm pulses from a Nd:YLF laser were used. Here we use 800 nm pulses from a Ti:sapphire laser. The main difference is a slightly lower absorption coefficient at 800 nm.[19] The 30 nm particle absorption cross-section $\sigma = 8 \times 10^{-13}$ cm^2 at 800 nm is 55% of the 1053 nm value.[19] As discussed below, the flash-heating fluence at the center of the laser beam was $J = 0.8$ J/cm^2. The energy input per unit volume of Al in the nanoparticle E_v is given by[7]

$$E_v = \frac{\rho J \sigma}{m_{Al}} \quad (1)$$

where $\rho = 2.6$ g/cm^3, and for 30 nm particles with a 2 nm oxide layer, $m_{Al} = 2.4 \times 10^{-17}$ g. Thus in our experiments, if adiabatic heating is assumed, $E_v = 70$ kJ/cm^3. The contribution due to exothermic chemistry is less than 21 kJ/cm^3. As a point of reference, vaporizing solid Al with slow heating requires $E_v = 31$ kJ/cm^3.[11] Deducing a temperature at the end of the pulse from E_v is a difficult problem that requires us to account for the heat capacity, exothermic chemistry, thermal conduction, volume expansion, ionization, and so forth. Using methods described elsewhere,[7] with additional confirmation by noticing the output emission spectrum is peaked in the visible, we believe the flash-heated Al is a weakly ionized plasma at a temperature of 4000−8000K.

C. Laser System. The laser system is diagrammed in Figure 3. It includes an 800 nm Ti:sapphire femtosecond oscillator (Kapteyn-Murnane) and a chirped pulse amplifier (Quantronix Titan).[24] The amplifier stretches the input pulse to ∼120 ps and sends the chirped pulse into a regenerative amplifier and a two-pass power amplifier operating at a repetition rate of 1 kHz prior to pulse compression to 150 fs. An optical chopper is used to reduce the repetition rate to 100 pps for compatibility with our sample rastering apparatus. We split off 30% of the pulse

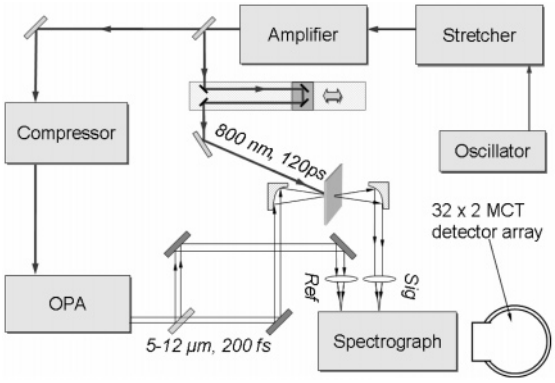

Figure 3. Schematic of Ti:sapphire laser system. The samples are flash-heated by stretched 120 ps duration 800 nm near-IR pulses and probed by femtosecond IR pulses generated by an optical parametric amplifier (OPA). The dual-beam IR system uses a 32 × 2 element HgCdTe (MCT) detector array.

prior to the compressor. This pulse with 120 ps duration travels down an optical delay line with a maximum range of 20 ns and is then used for flash heating. The data reported here used flash-heating pulse energies $E_p = 0.2$ mJ. The beam profile was roughly Gaussian with a (1/e^2) beam diameter at the sample surface of 250 μm. The IR system probes a region at the center of this beam where the intensity is approximately uniform. Assuming a Gaussian profile, the fluence at the beam center[7,11] $J_c = 2E_p/(\pi r_0^2) = 0.8$ J/cm^2. A single flash-heating pulse can ignite an energetic reaction in the confined Al/Teflon^{AF} sample, leaving an approximately round crater ∼200 μm in diameter, as shown in Figure 1.

The remainder of the laser pulse is compressed to 150 fs and used to pump an optical parametric amplifier (Light Conversion TOPAS 800/fs DFG1,2) to produce IR pulses of ∼200 fs duration. The IR pulses have a bandwidth of ∼150 cm^{-1}, and the center frequency can be tuned from 2.5 to 18 μm. In this range, the IR pulse energy varies from ∼30 μJ at the shortest wavelengths to ∼1 μJ at the longest wavelengths. The IR pulses are split into signal and reference beams. The signal beam is focused into the sample and recollimated by off-axis parabolic mirrors. The IR spot size in the sample is wavelength-dependent; at the longest wavelengths used here, ∼10 μm, the focused IR beam diameter was smaller than 150 μm.

Overlapping the IR and visible beams on the sample required care due to the noncollinearity of the beams and the long path variation (∼6 m) of the delay stage. Initial alignment was done using a 100-μm pinhole in between the two CaF_2 windows in the same plane as the Teflon^{AF} sample. With the sample stationary, one sample location was exposed to a stream of several flash-heating pulses, which drilled a hole into the sample. The sample was monitored with the aid of a long-range 10× optical microscope. The IR beam was aligned through this hole by maximizing the transmitted signal on the IR detection system. Then an iris pair was positioned in the path of the pump beam, and during data acquisition, when the delay stage was moved, the alignment of the flash-heating pulses were rechecked relative to these irises.

The IR detection system consists of an f/8 imaging spectrograph (Chromex) and a LN_2-cooled multichannel 32 × 2 element HgCdTe array (Infrared Associates) with associated electronics (IR-6416 multichannel laser pulse spectroscopy system from Infrared Systems Development Corp.) The signal and reference beams were focused onto the slit of the spectrograph at different heights so that each fell onto its own 32-element array.

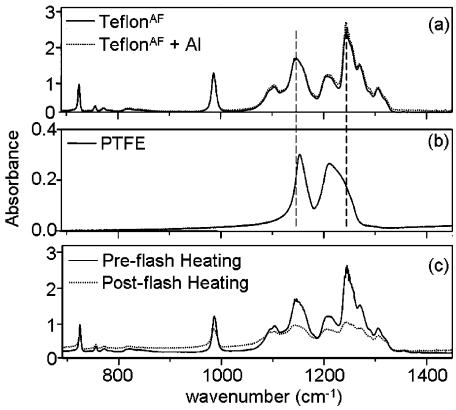

Figure 4. (a) IR spectra of Teflon^{AF} thin film with and without an 18 wt % load of Al nanoparticles. (b) IR spectrum of poly(tetrafluoroethylene) (PTFE). (c) FTIR spectra of Al-doped Teflon^{AF} films sandwiched between two IR windows, before and after flash heating.

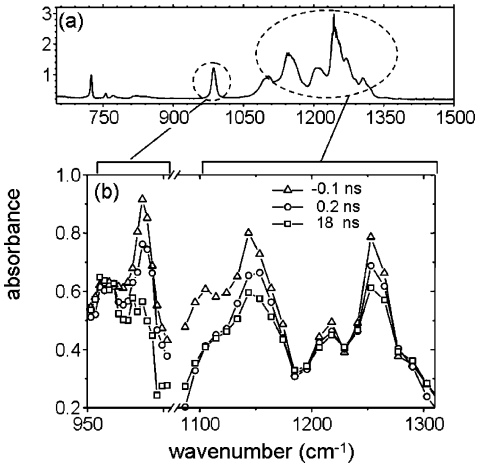

Figure 5. (a) FTIR spectrum of Al/Teflon^{AF} sample. The outlined regions are shown in detail below. (b) Time-resolved IR spectra at the indicated delay times. Near $t = 0$ the entire spectrum shows a broad underlying absorbance feature attributed to the Al plasma. As time progresses and Teflon^{AF} is consumed, the IR transitions lose absorbance.

3. Results

A. IR Spectroscopy of Teflon^{AF}. Figure 4 shows IR spectra of Teflon samples. Figure 4a shows spectra of a neat Teflon^{AF} sample and a Teflon^{AF} sample doped with 18 wt % Al nanoparticles. The nanoparticles and surfactant have negligible effect on the Teflon IR absorbance. Figure 4b is a spectrum we obtained using a PTFE tape, which agrees with published spectra[25] of PTFE. PTFE has two main bands associated with symmetric and asymmetric stretching of CF_2, at 1155 and 1220 cm^{-1}. The differences between PTFE and Teflon^{AF} are attributed to the dioxole groups in the latter. Our spectrum in Figure 4a appears identical to the spectrum denoted 66% mole fraction dioxole in Figure 2 of ref 26, so we believe that our Teflon^{AF} sample is a copolymer containing two dioxole units per TFE unit.

There remains some ambiguity in the assignment of the Teflon^{AF} bands. In this paper we are most interested in identifying spectral features that can be associated with either TFE or dioxole. The problem is that the stretching transitions for CF_2 of PTFE (1155 and 1220 cm^{-1}) and CFO of dioxole (1150 and 1245 cm^{-1}) are nearly coincident, as indicated by the dashed lines in Figure 4a,b, due to the small mass difference between O and F.[26] Bands of this sort in binary mixed crystals or binary copolymers having vibrational frequencies ν_a and ν_b and vibrational bandwidths $\Delta\nu_a$ and $\Delta\nu_b$ are usually described as being in either the *separated band* limit or the *amalgamation* limit.[27−31] The separated band limit occurs when the splitting $|\nu_a - \nu_b| \gg \Delta\nu$. In this case, copolymers have two separate transitions whose relative intensities reflect the composition. But CF_2 stretching of TFE and CFO stretching of dioxole are clearly in the amalgamation limit where $|\nu_a - \nu_b| \leq \Delta\nu$. In this case, as the composition is varied from pure TFE to pure dioxole, vibrational amplitude remains distributed over both moieties and only a single band is observed. The single band in the copolymer will range between the frequencies ν_a and ν_b. In the amalgamation limit, it is frequently the case that the frequency shift is a linear function of the composition, but this is not always true and more complicated concentration dependences such as quadratic dependences have been observed.[28,29]

Other Teflon^{AF} transitions of importance to this discussion are the 988 cm^{-1} band and the bands in the 1250 cm^{-1} range. The 988 cm^{-1} band is associated with dioxole and not TFE, and it originates from CF_3 stretching units of dioxole.[26] On the basis of relative spectral intensities and overlaps, the 1250 cm^{-1} band should be viewed as originating primarily from dioxole CFO stretching with a smaller contribution from asymmetric CF_2 stretching of TFE.

B. Fast IR with Flash Heating. A single flash-heating pulse ignites a sample volume about 200 μm in diameter and 3−4 μm thick (e.g., Figure 1), containing ∼100 ng of sample.[18] Associated with the ignition process is an audible snapping sound and a flash of light that can be seen by eye. The IR beam of our FTIR spectrometer is about 1 mm in diameter, so for one set of experiments we adjusted the speed of the positioner so that the flash-heating pulses overlapped in the sample. This allowed us to flash-heat a contiguous region large enough for FTIR measurements. Figure 4c shows the result. After flash heating, the Teflon^{AF} IR bands noticeably decrease in intensity, even though there is no possibility that the heated materials can escape the confinement of the IR window sandwich.

Figure 5 shows some representative time-resolved spectra at delays ranging from −0.1 to 18 ns. Time zero denotes the peak of the flash-heating pulse, so −0.1 ns is a time just prior to the onset of flash heating. These spectra were obtained in two separate runs, with the IR pulses tuned into the 1100−1300 cm^{-1} region or the 988 cm^{-1} region.

At shorter delay times when the flash heating pulse is present, and perhaps a little bit afterward, there is a broad and roughly featureless increase in the sample's mid-IR absorption. This broadband increase is attributed to a partially ionized Al plasma in the sample,[11,12] and since it has no clear association with the Al/Teflon reaction it will not be discussed further except to say that both the plasma absorption and the Teflon consumption by Al increased with increasing flash-heating fluence, and 0.8 mJ/cm^2 was chosen as the point of optimization where the ratio of Teflon absorbance change to plasma absorption was a maximum.

We analyzed our transient spectra by focusing on the 988, 1148, and 1250 cm^{-1} bands. We surveyed the 3.3−9 μm range to look for reaction products but were unable to find anything significant that stood out above the IR background from Al and Teflon^{AF}.

We subtracted the broad plasma contribution and determined the integrated band areas as a function of delay time, as plotted in Figure 6. These IR transients were normalized to an initial value of unity to give a Teflon^{AF} survival probability. In Figure 6, the peaked function centered at $t = 0$ is a Gaussian function with full width at half-maximum (fwhm) of 120 ps, which is

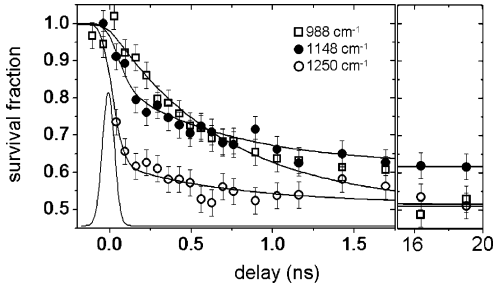

Figure 6. Time-dependent survival probability obtained from three Teflon^{AF} IR transitions. The smooth curves are a fit to eq 2, which assumes a faster and a slower exponential decay to a long-time plateau. The flash-heating pulse is 120 ps fwhm.

TABLE 1: Parameters Used to Fit the IR Absorption Transients in Figure 6 to Equation 2

wavenumber (cm^{-1})	*A* (amplitude of faster process)	*B* (amplitude of longer-time plateau)	$(k_1)^{-1}$, ps	$(k_2)^{-1}$, ns
988	0	0.5	50 (±20)	0.7 (±0.05)
1148	0.1	0.6	50 (±20)	0.7 (±0.05)
1250	0.35	0.5	50 (±20)	0.7 (±0.05)

the best fit to the experimentally determined cross-correlation between the 800 nm flash-heating pulses and the IR probe pulses. This curve represents the temporal response of the apparatus to an instantaneous process. Since the IR pulses are of femtosecond duration, the temporal response is determined by the duration of the flash-heating pulse. The transients in Figure 6 appear to level out to about half their initial value by 20 ns, which is the longest delay that can be achieved with our laser system. The FTIR data in Figure 3c, which were obtained a long time (1 h) after flash heating, appear consistent with the idea that the transients change very little after 20 ns. Approximately 50% consumption/survival of Teflon^{AF} after flash heating in a sample containing 18% Al is consistent with the discussion of stoichiometry in the Experimental Section.

The IR transients show both a faster and a slower decay. The 980 and 1148 cm^{-1} bands have a similar time dependences, but the 1250 cm^{-1} band is clearly different; it exhibits much more of the faster process than the others. The smooth curves in Figure 6 are the best fits to a phenomenological function having a biexponential decay with a long-time plateau:

$$I_i(t) = P(t) * [A_i \exp(-k_1 t) + (1 - A_i - B_i) \exp(-k_2 t) + B_i] \quad (2)$$

In eq 2, $P(t)$ represents the temporal envelope of the flash-heating pulse and * denotes convolution, A_i denotes the fraction of the decay associated with the faster process and B_i the amplitude of the long-time plateau, and k_1 and k_2 are the faster and slower rate constants. Equation 2 provides a good fit to the data in Figure 6 with one pair of constants A_i and B_i for each of the three transients and the same values of k_1 and k_2 for all three transients. Although the faster process is somewhat faster than the laser pulse duration, it was clearly slower than an instantaneous process, as seen by comparing the transient to the time integral of the apparatus temporal response function shown in Figure 6. Our best estimate of the faster time constant is $(k_1)^{-1} = 50$ (±20) ps. The slower time constant was $(k_2)^{-1} = 0.7$ (±0.1 ns). The values of the fitted parameters are summarized in Table 1.

A very interesting observation is an oscillation in the frequency shift of the IR transition near 1150 cm^{-1}. During the faster process this peak shifts to higher frequency, toward the 1155 cm^{-1} value associated with ambient PTFE. Then during the slower process the peak gradually returns back to 1148 cm^{-1}. The smooth curve through the data is the model discussed in the next section.

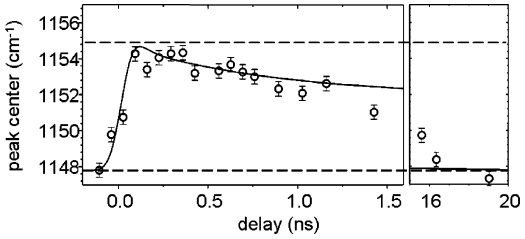

Figure 7. Frequency oscillation in the 1148 cm^{-1} vibration. Starting at the 1148 cm^{-1} value characteristic of Teflon^{AF}, the frequency shifts toward the TFE value with a 50 ps time constant and then back toward the Teflon^{AF} value with a 0.7 ns time constant. The smooth curve is calculated by use of a model where Al nanoparticles react faster with CFO than with CF_2.

4. Discussion

We begin with a brief summary. The Teflon^{AF} samples are 18 wt % of 30 nm Al, which by our estimate is enough to consume about half of the Teflon^{AF}. Three IR transitions, at 988, 1148, and 1250 cm^{-1}, were studied in detail. These transients were fit with a combination of a faster 50 ps process and a slower 0.7 ns process plus a long-time plateau. The 988 cm^{-1} transition is associated with CF_3 of dioxole and is not seen in TFE. This transient was the simplest, displaying solely a single 0.7 ns exponential decaying to a plateau of 0.5. The 1250 cm^{-1} transition is primarily sensitive to CFO stretching of dioxole with a lesser contribution from asymmetric CF_2 stretching of TFE. This transient also decays to a longer-time plateau of 0.5. About 70% of the decay is the faster 50 ps process and the remaining 30% is the slower 0.7 ns process. The 1148 cm^{-1} band is an amalgamated dioxole and PTFE excitation but we cannot confidently predict how its intensity varies with composition. This transient decays to a longer-time plateau of 0.6. About 25% of the decay is the faster 50 ps process and 75% is the slower 0.7 ns process. This band has an interesting time-dependent frequency oscillation shown in Figure 7. During the faster process the band blue-shifts in the direction of TFE, and during the slower process it red-shifts back toward the Teflon^{AF} value.

Taken together, these observations strongly support the idea that the faster process is the reaction of flash-heated Al with CFO of dioxole and the slower process is the reaction of Al with CF_2 or CF_3. If there is a difference in reaction rate of Al with CF_3 of dioxole or CF_2 of TFE, we could not distinguish it, but the reaction of Al with CFO (or quite possibly just the O atoms themselves) is clearly more than 10 times faster than the reaction of Al with the F atoms.

The 1148 cm^{-1} frequency shift oscillation can be explained in terms of a time-varying composition of the Teflon shell around each nanoparticle. Certainly a part of the total frequency shift should be attributed to the transient high temperatures and pressures in the sample. But we believe composition is more important because the other IR transitions subject to the same temperature and pressure effects do not show such a frequency oscillation. In our view, the faster initial blue shift results from fast consumption of CFO of dioxole in the shells surrounding the Al nanoparticles, which makes the sample temporarily rich in PTFE. The slower red shift results from subsequent consumption of CF_2 of TFE in the same shells. Once both the

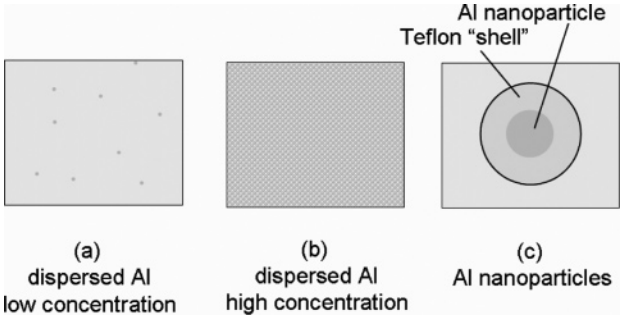

Figure 8. Three motifs for the reaction of Al fuel with a Teflon^{AF} oxidizer. (a) Individual Al atoms are dispersed throughout the oxidizer at a low concentration. (b) Individual Al atoms are dispersed throughout the oxidizer at a concentration sufficient to consume all the oxidizer. (c) Al nanoparticles dispersed in the oxidizer creates two regions of oxidizer, a shell of oxidizer surrounding the nanoparticle where the local fuel concentration is high and a region of oxidizer with no fuel.

CFO and CF_2 components of these shells are completely consumed, the sample composition is that of the unreacted Teflon^{AF} that was distant from the Al nanoparticles.

It is worthwhile to emphasize that such an oscillation is a consequence of the segregation of fuel and oxidizer on the nanoscale, and we will now show this using a simplified model that replicates the effects we observe without a complete treatment of the complicated chemical reaction mechanisms. This is a model with Al fuel plus two types of oxidizers B and C, where B (e.g., CFO) reacts with Al much more rapidly (about 10 times faster) than the less reactive C (e.g., CF_2). We will use this model to calculate time concentrations and frequency shifts with three different motifs of Al dispersion, as depicted in Figure 8. Figure 8 panels a and b show hypothetical cases with no nanostructure. Here individual Al atoms are dispersed throughout the Teflon^{AF}. In Figure 8a the Al concentration is low so the nanoenergetic material is Teflon-rich. In Figure 8b there is a stoichiometric balance between Al and Teflon^{AF}, so all the fuel and oxidizer can be consumed. Figure 8c corresponds to the nanostructured energetic materials studied here. There are effectively two types of oxidizer present. The first type is located in the shell surrounding each Al nanoparticle, and it is completely consumed by reactions with the nanoparticle. The second type is distant from the nanoparticles and does not react at all.

The chemical kinetics in all three motifs can be described by the following scheme:

$$
\begin{aligned}
-\frac{\mathrm{d}[Al(t)]}{\mathrm{d}t} &= k_1[Al(t)][B(t)] + k_2[Al(t)][C(t)] \\
-\frac{\mathrm{d}[B(t)-B_0]}{\mathrm{d}t} &= k_1[Al(t)][B(t)] \\
-\frac{\mathrm{d}[C(t)-C_0]}{\mathrm{d}t} &= k_2[Al(t)][C(t)]
\end{aligned}
\tag{3}
$$

In eq 3, the effects of Al nanostructure are incorporated in the terms B_0 and C_0. The purpose of introducing these parameters is to simulate the correct final state of the oxidizer. The fraction of the oxidizer components B and C that is distant from the nanoparticles cannot react with Al; this fraction is characterized by B_0 and C_0. The fractions $B(t = \infty)$ and $C(t = \infty)$ are independent of B_0 and C_0: the first set represents the solution of eq 3 without the B_0 and C_0 terms, whereas the second is the fraction of oxidizer that did not participate in the reaction.

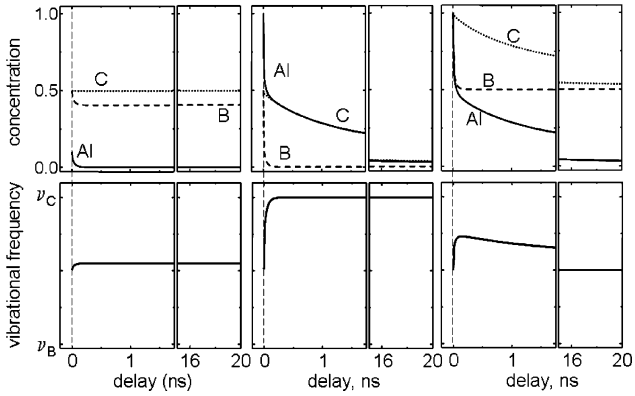

Figure 9. (Upper panels) Results from the kinetic model eq 3, where Al fuel can react with a two-component oxidizer consisting of a faster-reacting B and a slower-reacting C component. (Lower panels) Time-dependent frequency shift of an amalgamated vibration whose frequency is described by eq 4. The three pairs of upper and lower panels correspond to the three physical situations depicted in Figure 8.

To compute the frequency shift, we consider a vibrational transition of A and B that is amalgamated in the copolymer, and we assume for simplicity that the shift is a linear function of concentration. Let ν_B be the vibrational frequency of oxidizer B and ν_C the frequency of oxidizer C. The frequency of the amalgamated vibration at any instant is given by

$$
\begin{aligned}
\nu &= \nu_B + \chi_C(\nu_C - \nu_B) \\
\chi_C &= \frac{C(t) + C_0}{B(t) + B_0 + C(t) + C_0}
\end{aligned}
\tag{4}
$$

The results of this model for the case described in Figure 8a, where only a small fraction of the oxidizer is consumed, are shown in Figure 9 (left panels). We used the parameters $[Al(t = 0)] = 0.1$, $[B(t = 0)] = 0.5$, $[C(t = 0)] = 0.5$, and $B_0 = C_0 = 0$. There is just enough Al present to consume 10% of the total (B + C) oxidizer present and no nanostructure. Figure 9 (left panels) shows the Al disappearance occurs with an ~50 ps time constant. Most of this Al is consumed in reactions with B; very little Al is consumed by the slower-reacting C. Initially the vibrational frequency of the oxidizer copolymer is the frequency corresponding to $\chi_C = 0.5$, which is $(\nu_B + \nu_C)/2$. After a few multiples of 50 ps, the oxidizer has lost a small fraction of its B component and hardly any of its C component, so the vibrational frequency evidence a small but rapid shift from $(\nu_B + \nu_C)/2$ toward the value ν_C.

The results for the case depicted in Figure 8b, where there is no nanostructure but enough Al to consume all the (B + C) oxidizer, are shown in Figure 9 (center panels). We used the parameters $[Al(t = 0)] = 1.0$, $[B(t = 0)] = 0.5$, $[C(t = 0)] = 0.5$, and $B_0 = C_0 = 0$. Figure 9 (center panels) shows a rapid reaction between Al and the B oxidizer consumes about half of the Al and almost all of the B oxidizer. Subsequently the slower reaction between Al and the C oxidizer consumes the remaining Al and all the C oxidizer. Initially the frequency is $(\nu_B + \nu_C)/2$. As the B oxidizer disappears, the frequency shifts toward ν_c. Once almost all the B oxidizer has been consumed, which occurs in a few multiples of 50 ps, the last trace of oxidizer is almost pure C and the frequency goes asymptotically to the value ν_C.

The results of this model for the case described in Figure 8c with Al nanostructure are shown in Figure 9 (right panels). We took $[Al(t = 0)] = 1.0$, $[B(t = 0)] = 0.5$, $[C(t = 0)] = 0.5$, and $B_0 = C_0 = 0.5$. In other words, half of the (B + C) oxidizer can react with Al and the other half cannot. The half that reacts

is located in shells surrounding the Al nanoparticles. Figure 9 (right panels) shows a fast consumption of the part of the B oxidizer that can react with Al, leading to a fast shift from the frequency $(\nu_B + \nu_C)/2$ toward the frequency ν_C. The subsequent slower reaction consumes the part of the C oxidizer that can react with Al, leading to a slower shift back to the initial value $(\nu_B + \nu_C)/2$. This is the frequency oscillation observed in Figure 7, and the smooth curve that fits the data in Figure 7 was calculated from eqs 3 and 4, where $(\nu_B + \nu_C)/2 = 1148$ cm^{-1} and $\nu_C = 1162$ cm^{-1}. These wavenumber values differ slightly from what could be derived from ambient IR spectra of pure PTFE or pure dioxole,[26] presumably because the time-dependent measurements involve high temperatures and pressures.

5. Conclusions

Using ultrafast IR spectroscopy, we have studied the reactions between flash-heated Al nanoparticles and Teflon^{AF}. In our interpretation of the Teflon^{AF} spectrum, we assigned one IR band to CF_3 stretching, one to CFO stretching, and one IR band to represent an amalgamated vibration having amplitude on both CF_2 and CFO. The reactions of Al with CF_2 and CF_3 have the same apparent rate, so it proved possible to describe the Al + Teflon^{AF} chemistry with just two processes, the slower involving Al + CF_2 or CF_3 and the faster involving Al + CFO. The reactions with CFO were more than 10 times faster than reactions with CF_2 or CF_3. An unusual observation was a time-dependent oscillation in the frequency of the amalgamated vibration after flash heating. Starting at 1148 cm^{-1}, this vibration shows an ~100 ps shift to 1154 cm^{-1} followed by a more gradual nanosecond shift back to 1148 cm^{-1}.

We have successfully modeled the IR transients and the frequency oscillation using a kinetic model where Al fuel can react with a binary oxidizer system B + C, where the reaction with B is about 10 times faster than the reaction with C. The nature of fuel-oxidizer chemistry in such a binary oxidizer system can be quite dependent on the fuel-to-oxidizer ratio. When the system is oxidizer-rich, the Al reacts almost entirely with B; when the fuel-oxidizer ratio is balanced, B is consumed first and then C is consumed. Neither of these schemes replicates the frequency oscillation we saw, but when the Al fuel was spatially segregated in the form of nanoparticles, there were both regions of high local concentrations of fuel and regions with no fuel. In this case our kinetic model outputs a frequency oscillation that fit the observations very well.

Acknowledgment. The research described in this publication is based on work supported by the U.S. Air Force Office of Scientific Research under Award FA9550-06-1-0235 and the U.S. Army Research Office under Contract W911NF-04-1-0178. Thin film measurements were carried out in the Center for Microanalysis of Materials, University of Illinois at Urbana−Champaign, which is partially supported by the U.S. Department of Energy under Grant DEFG02-91-ER45439. We gratefully acknowledge the work of Hyunung Yu, who obtained the images shown in Figure 2.

References and Notes

(1) *Synthesis, Characterization and Properties of Energetic/Reactive Nanomaterials*; Armstrong, R. W., Thadhani, N. N., Wilson, W. H., Gilman, J. J., Munir, Z., Simpson, R. L., Eds.; Materials Research Society: Warrendale, PA, 2004; Vol. 800.

(2) Fried, L. E.; Manaa, M. R.; Pagoria, P. F.; Simpson, R. L. *Annu. Rev. Mater. Res.* **2001**, *31*, 291.

(3) Dlott, D. D. *Mater. Sci. Technol.* **2006**, *22*, 463.

(4) *Overviews of recent research on energetic materials*; Thompson, D., Brill, T., Shaw, R., Eds.; World Scientific: River Edge, NJ, 2005.

(5) *Multifunctional Energetic Materials*; Thadhani, N. N., Armstrong, R. W., Gash, A. E., Wilson, W. H., Eds.; Materials Research Society: Warrendale, PA, 2005.

(6) Wang, S.; Yang, Y.; Yu, H.; Dlott, D. D. *Propellants, Explos., Pyrotech.* **2005**, *30*, 148.

(7) Yang, Y.; Wang, S.; Sun, Z.; Dlott, D. D. *J. Appl. Phys.* **2004**, *95*, 3667.

(8) Yang, Y.; Sun, Z.; Wang, S.; Hambir, S. A.; Yu, H.; Dlott, D. D. Ultrafast spectroscopy of laser-initiated nanoenergetic materials. In *Synthesis, Characterization and Properties of Energetic/Reactive Nanomaterials, MRS Symposium Proceedings*; Armstrong, R. W., Thadhani, N. N., Wilson, W. H., Gilman, J. J., Munir, Z., Simpson, R. L., Eds.; Materials Research Society: Warrendale, PA, 2004; Vol. 800, pp 151.

(9) Wang, S.; Yang, Y.; Sun, Z.; Dlott, D. D. *AIP Conf. Proc.* **2004**, *706*, 1065.

(10) Dlott, D. D.; Yu, H.; Wang, S.; Yang, Y.; Hambir, S. A. Nanotechnology energetic material dynamics studied with nanometer spatial resolution and picosecond temporal resolution. In *Advances in Computational & Experimental Engineering & Sciences '04*; Atlurl, S. N., Tadeu, A., Eds.; Tech Science Press: Madeira, 2004; pp 1427.

(11) Yang, Y.; Sun, Z.; Wang, S.; Dlott, D. D. *J. Phys. Chem. B* **2003**, *107*, 4485.

(12) Wang, S.; Yang, Y.; Sun, Z.; Dlott, D. D. *Chem. Phys. Lett.* **2002**, *368*, 189.

(13) Parker, L. J.; Ladouceur, H. D.; Russell, T. P. *AIP Conf. Proc.* **2000**, *505*, 941.

(14) Yu, H.; Dlott, D. D.; Kearney, F. R. *J. Imag. Sci. Technol.* **2006**, *50*, 401.

(15) Yu, H.; Hambir, S. A.; Dlott, D. D. Ultrafast dynamics of nanotechnology energetic materials. In *Multifunctional Energetic Materials*; Armstrong, R. W., Thadhani, N. N., Wilson, W. H., Gash, A. E., Munir, Z., Eds.; MRS Symposium Proceedings; Materials Research Society: Warrendale, PA, 2006; Vol. 896, p 0896.

(16) Tolbert, W. A.; Lee, I.-Y. S.; Wen, X.; Doxtader, M. M.; Ellis, E. W.; Dlott, D. D. *J. Imag. Sci. Technol.* **1993**, *37*, 485.

(17) Zel'dovich, Y. B.; Raiser, Y. P. *Physics of Shock Waves and High-temperature Hydrodynamic Phenomena*; Academic Press: New York, 1966.

(18) Yang, Y.; Wang, S.; Sun, Z.; Dlott, D. D. *Appl. Phys. Lett.* **2004**, *85*, 1493.

(19) Yang, Y.; Wang, S.; Sun, Z.; Dlott, D. D. *Propellants, Explos., Pyrotech.* **2004**, *30*, 171.

(20) Kim, H.; Hambir, S.; Dlott, D. D. *Shock Waves* **2002**, *12*, 79.

(21) Kim, H.; Hambir, S. A.; Dlott, D. D. *Phys. Rev. Lett.* **1999**, *83*, 5034.

(22) Kim, H.; Hambir, S. A.; Dlott, D. D. *J. Phys. Chem. B* **2000**, *104*, 4239.

(23) Bohren, C. F.; Huffman, D. R. *Absorption and Scattering of Light by Small Particles*; John Wiley and Sons: New York, 1998.

(24) Fu, Q.; Seier, F.; Gayen, S. K.; Alfano, R. R. *Opt. Lett.* **1997**, *22*, 712.

(25) Schrader, B. *Raman/Infrared Atlas of Organic Compounds*, 2nd ed.; VCH: Weinheim, Germany, 1989.

(26) Nason, T. C.; Lu, T.-M. *Thin Solid Films* **1994**, *239*, 27.

(27) Ziman, J. M. *Models of disorder. The theoretical physics of homogeneously disordered systems*; Cambridge University Press: Cambridge, U.K., 1979.

(28) Chronister, E. L.; Dlott, D. D. *J. Chem. Phys.* **1983**, *79*, 5286.

(29) Velsko, S.; Hochstrasser, R. M. *J. Phys. Chem.* **1985**, *89*, 2240.

(30) Prasad, P. N.; Kopelman, R. *J. Chem. Phys.* **1972**, *57*, 863.

(31) Prasad, P. N.; Kopelman, R. *J. Chem. Phys.* **1972**, *57*, 856.